sustainability

MDPI

Article

Poisonous Vapor Adsorption on Pure and Modified Aluminum Nitride Nanosheet for Environmental Safety: A DFT Exploration

Hongni Zhang [1,2], Wenzheng Du [1], Tong Zhao [1], Rajeev Ahuja [3,4] and Zhao Qian [1,*]

1 Key Laboratory of Liquid-Solid Structural Evolution and Processing of Materials (Ministry of Education), School of Management, Shandong University, Jinan 250061, China; nini810@126.com (H.Z.); 201813740@mail.sdu.edu.cn (W.D.); zhaotgc@163.com (T.Z.)
2 College of Industry and Commerce, Shandong Management University, Jinan 250357, China
3 Condensed Matter Theory, Department of Physics and Astronomy, Ångström Laboratory, Uppsala University, 75120 Uppsala, Sweden; rajeev.ahuja@physics.uu.se
4 Applied Materials Physics, Department of Materials Science and Engineering, KTH Royal Institute of Technology, 10044 Stockholm, Sweden
* Correspondence: qianzhao@sdu.edu.cn

Received: 14 November 2020; Accepted: 1 December 2020; Published: 3 December 2020

Abstract: Through Density Functional Theory (DFT), we have unveiled the atomic structures, adsorption characteristics and electronic structures of the poisonous and explosive vapor, m-dinitrobenzene (m-DNB), on pure, defective and various doped AlN nanosheets from a physical perspective. It is found that the adsorption energy, band gap change and sensitivity to the vapor are significantly increased through atomic-scale modification of the nanosheet. The AlN monolayer with Al-N divacancy has the largest adsorption energy and has potential to be utilized as adsorption or filtration materials for m-DNB vapor. The Si-doped AlN nanosheet possesses a much larger band gap change (−0.691 eV) than the pure nanosheet (−0.092 eV) after adsorption and has a moderate adsorption energy, which could be candidate material for explosive vapor sensing. This theoretical work is proposed to provide guidance and clue for experimentalists to develop more effective two-dimensional materials for environmental safety and sustainability.

Keywords: poisonous vapor; environmental safety; health; sustainability; m-DNB; AlN nanosheet

1. Introduction

In recent years, two-dimensional materials have been developing rapidly. A large number of materials, such as graphene [1,2], silicene [3,4], phosphorene [5], boron nitride [6,7] and metal dichalcogenides [8], are widely studied in various fields in terms of their unique electronic structures and physical properties. Due to the high specific surface area and designability of some two-dimensional materials, they have great potential in the field of molecular sensing and gas adsorption [9–13]. In the early days, a lot of research works studied graphene-based materials using experiments or theory, but they had certain limitations due to the lack of band gap [14–19]. In order to obtain more ideal sensing or filtering systems, the adsorption properties of other two-dimensional materials have been explored.

The aluminum nitride (AlN) nanosheet is a kind of two-dimensional material with a wide indirect band gap. Zhang et al. used aluminum powder and ammonia to prepare smooth, uniform, and high-yield single crystal AlN nanosheets on the silicon substrate by a vapor transmission method [20]. Some researchers have theoretically studied the properties of pure AlN nanosheets, including geometric structure [21], electronic structure [22], optical [23] and magnetic [24] properties. It is also found that

AlN nanosheets have good sensing performance for toxic gases such as CO, NO, SO_2 and NO_2 [25–28]. Like other two-dimensional materials, the properties of the AlN nanosheet can be greatly changed through modification, such as doping, decoration or vacancy-making [29–31]. Ouyang et al. has found that the single-layer AlN with vacancy defects has strong interaction with SO_2 and NO_2 molecules, and it is a promising candidate for adsorption or filtration materials [32].

M-Dinitrobenzene (m-DNB) is a kind of organic compound usually used as a raw material for synthetic dyes, pesticides and explosives, as well as analytical reagents in chemical industry [33–36]. However, the matter is volatile and the vapor can easily explode. The vapor is also highly toxic when inhaled and in contact with the skin, which brings danger to human health and environment. Thus, it is crucial to detect the trace level of this vapor evolved from the explosive material and the sensitive detection of this trace vapor is particularly important. Besides the traditional methods and sensing materials, such as metal oxides, microcantilevers and polymer materials, some low-dimensional materials, especially 2D nanomaterials with large specific surface areas, and rich active sites are opening the inroads for their possible application in explosive detection [37]. For example, R. Chandiramouli et al. used a pure single-layer antimony sheet to study the detection of explosive vapors, which had fast response and selectivity. In addition, a few other researchers explored the adsorption behavior of the poisonous and explosive m-DNB vapor on 2D nanosheets. In this work, we used Density Functional Theory (DFT) to explore the adsorption and sensing capabilities of m-DNB molecules on various pure, vacancy-defective (Al, N or Al-N dual vacancies) and M-doped (M = C, Mg, Si, P, Ti) AlN monolayers, revealing the potential of these nanomaterials from their electronic origin. It is not only significant to help screen potential candidate nanomaterials for next-generation chemical sensors towards explosive volatiles, but also meaningful to provide theoretical guidance for experimental researchers to develop more efficient two-dimensional sensing materials in general in the future.

2. Methods

The Density Functional Theory (DFT) calculations of various AlN nanosheets adsorbing m-DNB molecule were performed with Vienna Ab initio Simulation Package [38–42]. The generalized gradient approximation (GGA) with Perdew–Burke–Ernzerhof (PBE) [43] for exchange-correlation functional and the projector augmented wave (PAW) [44] method for electron–ion interactions with 520 eV cutoff energy were utilized. The integration of the Brillouin-zone was performed by using $5 \times 5 \times 1$ Monkhorst-Pack mesh during geometry optimizations and $15 \times 15 \times 1$ mesh for electronic structure calculations [45]. In order to avoid the interaction between adjacent layers due to periodicity, a vacuum space of 20Å was set in the *z*-axis direction. The van der Waals interactions were described using the Grimme's DFT-D2 approach [46]. For all calculations, the energy and force convergence criteria were set to 10^{-4} eV and 0.02 eV/Å, respectively. The adsorption energy (E_{ad}) of the m-DNB molecule on various AlN nanosheets was calculated by:

$$E_{ad} = E_{(AlN+m\text{-}DNB)} - E_{AlN} - E_{m\text{-}DNB} \quad (1)$$

where $E_{AlN+m\text{-}DNB}$ is the total energy of the optimized AlN nanosheets adsorbing m-DNB molecule, E_{AlN} and $E_{m\text{-}DNB}$ are the energies of bare AlN nanosheets and isolated m-DNB molecule, respectively.

3. Results and Discussion

3.1. Interaction of m-DNB Molecule with Pure AlN Nanosheet

Firstly, we have studied the adsorption behavior of m-Dinitrobenzene on the surface of pure AlN nanosheet to explore their physical interaction and figure out whether the pure substrate can effectively adsorb or sense this poisonous and explosive vapor. We have made an optimized $5 \times 5 \times 1$ supercell as the base material and the average Al-N bond length is 1.799 Å, which is consistent with the results of other theoretical work [47]. Next, the most stable adsorption configuration(s) of m-DNB on the surface of pristine AlN nanosheet have been explored. The m-DNB vapor molecule is

placed at various positions of the substrate in Figure 1. Considering that the different directions of the benzene ring will affect the interaction between the surrounding nitro group and AlN monolayer, there are two different parallel placement methods: direction of the benzene ring and hexagon of the matrix are the same (Figure 1a–c) or vertical (Figure 1d–f). Complete structural optimizations were carried out to evaluate their relative stability by calculating the adsorption energy. The optimized geometric structures, the corresponding energy and adsorption parameter results are shown in Table 1. The adsorption distance represents the minimum distance between the atom in the m-DNB molecule and the Al or N atom of the AlN nanosheet. The results show that, when m-DNB is placed in parallel on a pure AlN nanosheet, the adsorption energy is larger. Among them, when the Al-N bond is in the center of the benzene ring and the benzene ring is in the vertical direction with the AlN nanosheet's hexagon, the adsorption energy is the largest (−0.903 eV) with the most stable adsorption configuration shown in Figure 1f.

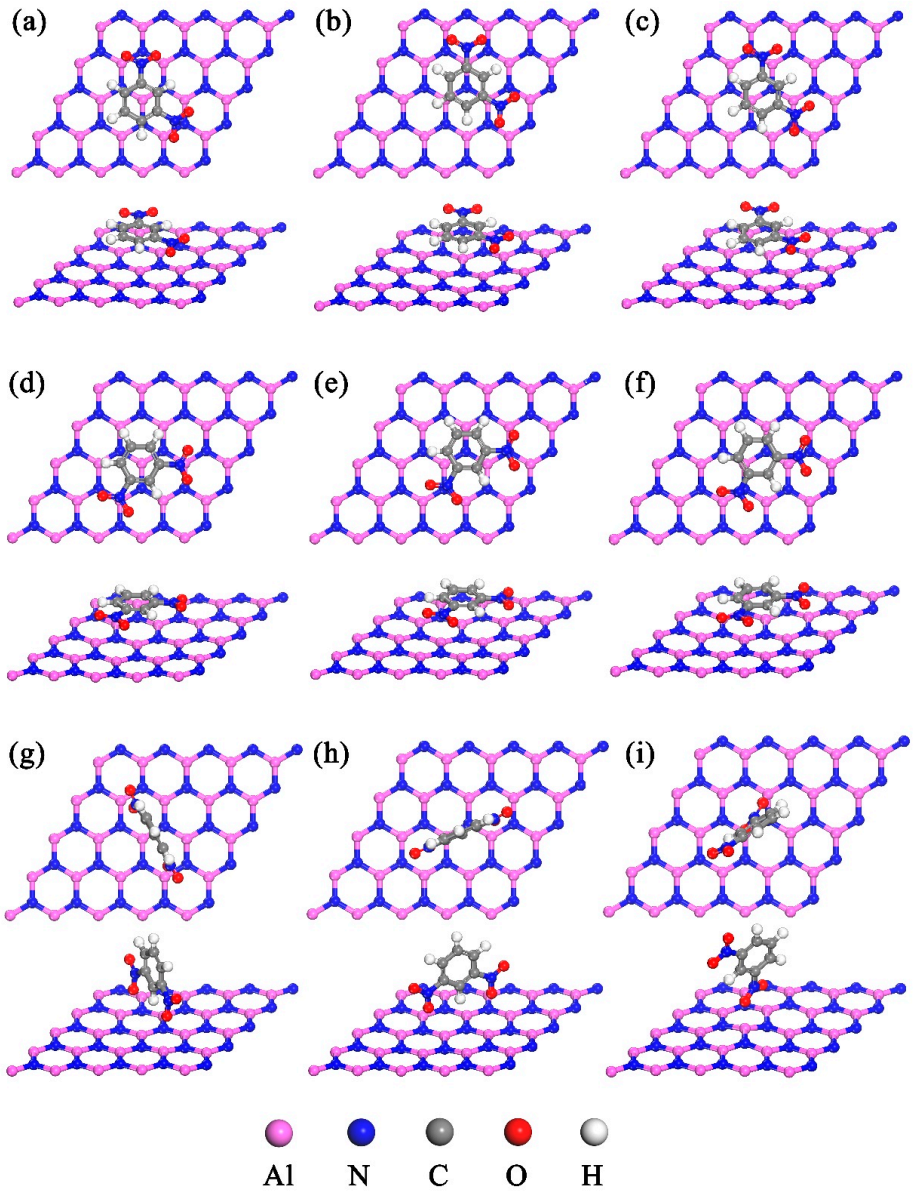

Figure 1. Optimized structures of different adsorption positions of m-DNB molecule on pure AlN nanosheet. (**a**–**f**) m-DNB is placed in parallel on pure AlN nanosheet; (**g**–**i**) m-DNB is perpendicular to pure AlN nanosheet. The purple, blue, gray, red and white balls denote the Al, N, C, O and H atoms, respectively.

Table 1. The adsorption energy and adsorption distance of m-DNB molecule on pure AlN nanosheet at different adsorption positions.

Configuration	a	b	c	d	e	f	g	h	i
E_{ad} (eV)	−0.806	−0.799	−0.742	−0.717	−0.901	−0.903	−0.649	−0.646	−0.829
d (Å)	3.270	3.212	3.254	3.340	3.029	2.924	2.602	2.962	2.083

From Table 1, it can be seen that the absolute value of adsorption energy of the most stable configuration is less than 1.0 eV. The corresponding adsorption distance is about 2.92 Å, which is the shortest among all parallel configurations. The change in m-DNB molecule is also not obvious. The pristine length of the N-O bond is 1.239 Å, which is stretched to 1.246 Å after being adsorbed on pure AlN nanosheet and the adjacent C-N bond is shortened from pristine 1.488 Å to 1.474 Å.

To further understand the adsorption properties of m-DNB on AlN nanosheet, the electronic structures have been calculated. In the differential charge density, shown in Figure 2, the charge transfer between the m-DNB molecule and pure AlN nanosheet is mainly concentrated in the nitro part; especially, there is a large amount of charge accumulation around the oxygen atom, and only a small part exists near the benzene ring. The Bader charge analysis accurately calculates that only 0.129 e^- charges are transferred to the m-DNB molecule. Figure 3 depicts the TDOS and PDOS of the pure AlN nanosheet before and after the adsorption of the m-DNB vapor molecule. The positions of the valence band and conduction band after adsorption are nearly unchanged, but the deep energy level is occupied in the forbidden band. It is calculated that the band gap change before and after adsorption is very small: the values are 2.704 eV and 2.612 eV, respectively. In PDOS, there is no obvious hybridization between the Al-p orbital of AlN nanosheet and the C-p and O-p orbitals of the m-DNB molecule, which also proves that the interaction between the molecule and the pure AlN substrate is not strong.

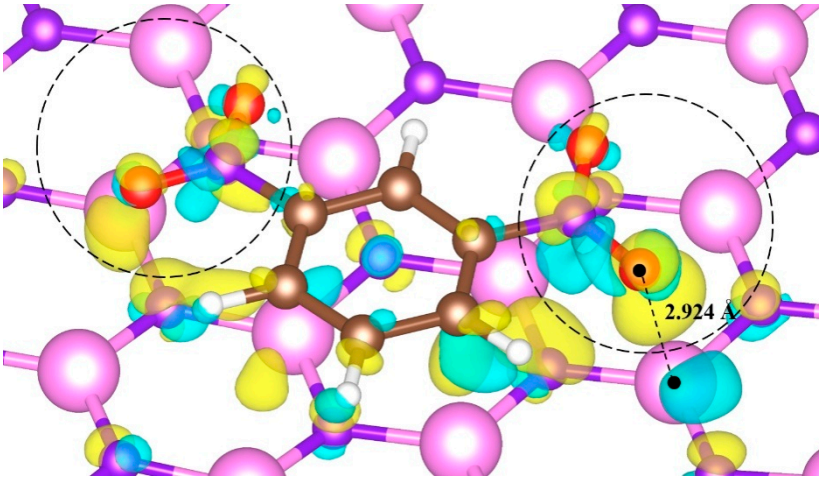

Figure 2. Differential charge density of m-DNB molecule adsorbed on pure AlN nanosheet. The isovalue of charge density is 0.0006 e/Å^3 (yellow: charge accumulation; cyan: charge depletion).

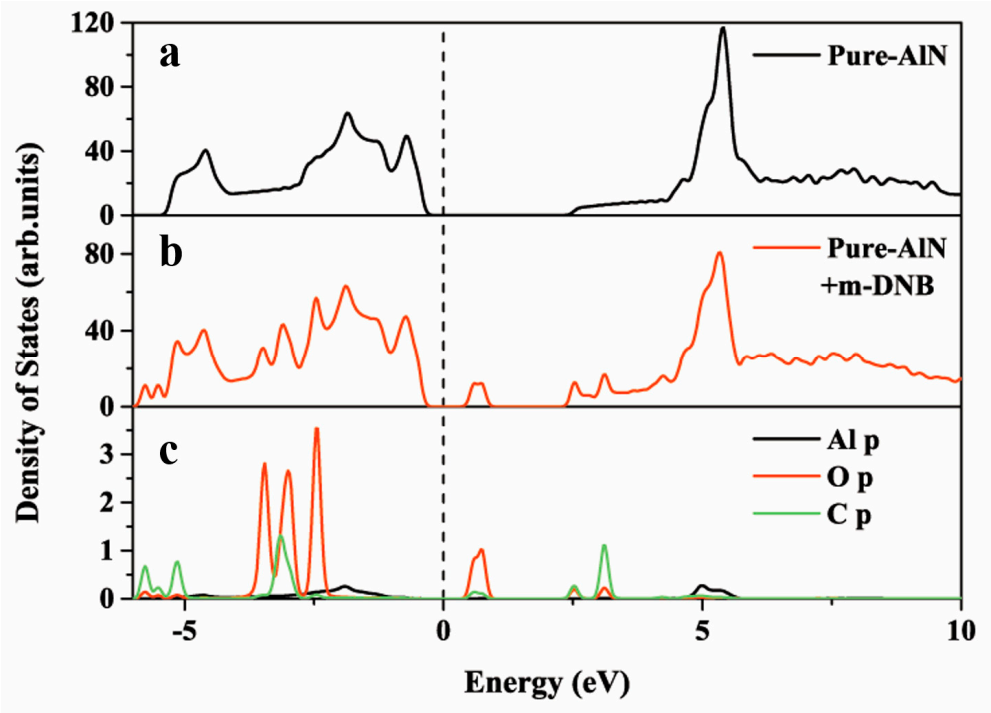

Figure 3. Electronic density of states of pure AlN nanosheet before and after m-DNB adsorption. (**a**) TDOS of pure AlN monolayer; (**b**) TDOS of monolayer after m-DNB molecule is adsorbed; (**c**) PDOS of O and C atom in m-DNB and the neighboring Al atom in AlN. The Fermi energy is set to zero.

In general, the adsorption of the m-DNB molecule on the pure AlN nanosheet is between physical adsorption and weak chemical adsorption. While, it is even worse that the small change in band gap before and after molecule adsorption will make the pure AlN nanosheet extremely insensitive to m-DNB and is not sufficient to be a sensing substrate for this poisonous and explosive vapor. Thus followingly, we have modified the AlN nanosheet by designing vacancies or doping to improve its adsorption and sensing performance towards m-DNB. Figure 4 shows the schematic band gap change and adsorption energy comparison of various modified AlN nanosheets for m-DNB adsorption and Table 2 gives the quantitative values. It is found that the AlN nanosheet with Al-N dual vacancies has the largest adsorption energy and the Si-doped AlN nanosheet has the largest band gap change and advantageous adsorption energy. As would be discussed in the following section, the nanosheet with Al-N-vacancies could greatly enhance the interaction between m-DNB and substrate due to the existence of dual vacancies and the adsorption energy is much larger than other configurations. However, for sensing application, the molecule is not easy to desorb from this substrate after adsorption and it could poison the surface of the material; thus, this system is more suitable as a kind of adsorption or filtration material. The relatively moderate adsorption energy brought by the Si-doped AlN nanosheet, as well as its largest band gap change after m-DNB adsorption, could make the system very likely to be used as a candidate for the vapor sensing application. It is true that the Al-vacancy or C-doped system also has medium binding energy, but for gas sensing application it is proposed that the band gap change should be as large as possible after molecule adsorption in order to obtain the electronic signal as optimally as possible. For this, it is not be hard to understand why the Ti-doped system with the band gap change of only −0.180eV will not be considered in the following detailed study. In the following two sections, we will focus on the Al-N-vacancies system (for adsorption or filtration application) and the Si-doped system (for sensing application) and investigate their atomic and electronic structures, respectively.

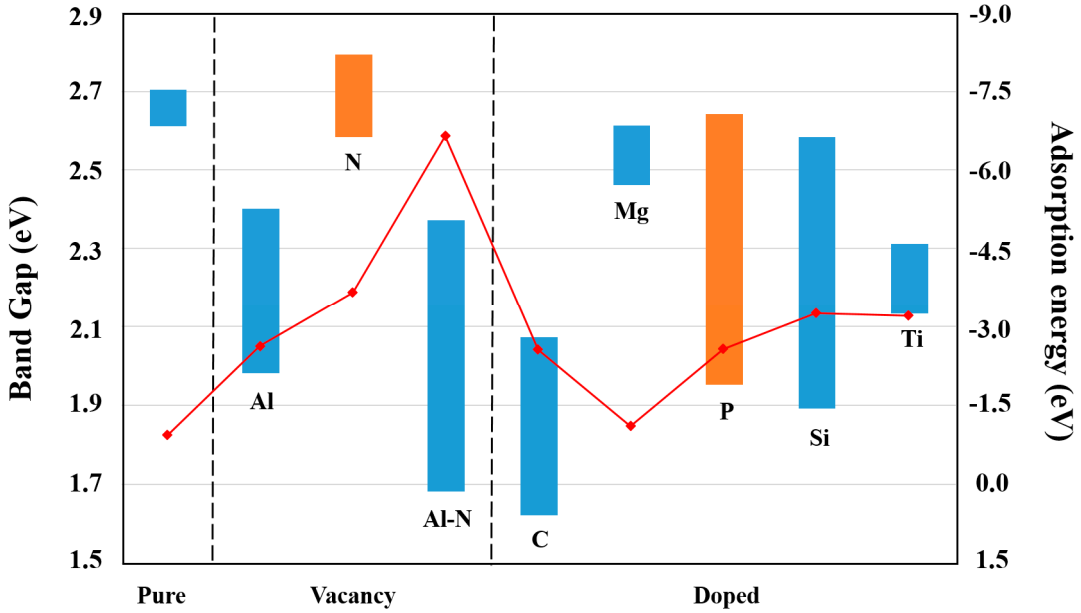

Figure 4. The band gap change range and adsorption energy curve of various modified AlN nanosheets for m-DNB adsorption. The band gap change uses the left ordinate, the blue bar represents the band gap decrease after m-DNB adsorption and the red bar represents the band gap increase. The adsorption energy uses the right ordinate, and the curve is marked with a red polyline.

Table 2. The adsorption energy (E_{ad}), adsorption distance and band gap change in various modified AlN nanosheets before and after m-DNB adsorption.

Systems	E_{ad} (eV)	Adsorption Distance (Å)	Band Gap Change (eV)
Pure	−0.903	2.924	−0.092
Al-vacancy	−2.693	1.463	−0.420
N-vacancy	−3.790	1.870	0.210
Al-N-vacancies	−6.957	1.495	−0.690
C-doped	−2.623	1.895	−0.452
Mg-doped	−1.083	2.399	−0.151
P-doped	−2.633	2.590	0.690
Si-doped	−3.360	2.019	−0.691
Ti-doped	−3.310	2.012	−0.180

3.2. Adsorption of m-DNB Molecule on AlN Nanosheet with Al-N Vacancies

First, we constructed a model of dual-vacancy AlN nanosheet. After the structure was relaxed, it was found that the N atoms near Al-vacancy contracted away from the vacancy and the adjacent Al-N bond length was shortened by 0.01 ~ 0.02 Å. The result near the N-vacancy is the opposite. The whole system was not significantly deformed and all the atoms remained in the same plane. The atomic structure and bond length are shown in Figure 5a. As is the case in the pure AlN nanosheet, the m-DNB molecule is placed at nine different initial sites and are all optimized. It was found that the most stable configuration was the m-DNB molecule adsorbed on the substrate obliquely. The atoms near the vacancies were obviously deformed and the nanosheet was bent upward as a whole. The O atom of the nitro group and the C atom of the benzene ring formed bonds with the Al and N atoms of the nanosheet, respectively. Three Al-O bonds and two C-N bonds were formed and the bond lengths have been marked in Figure 5b.

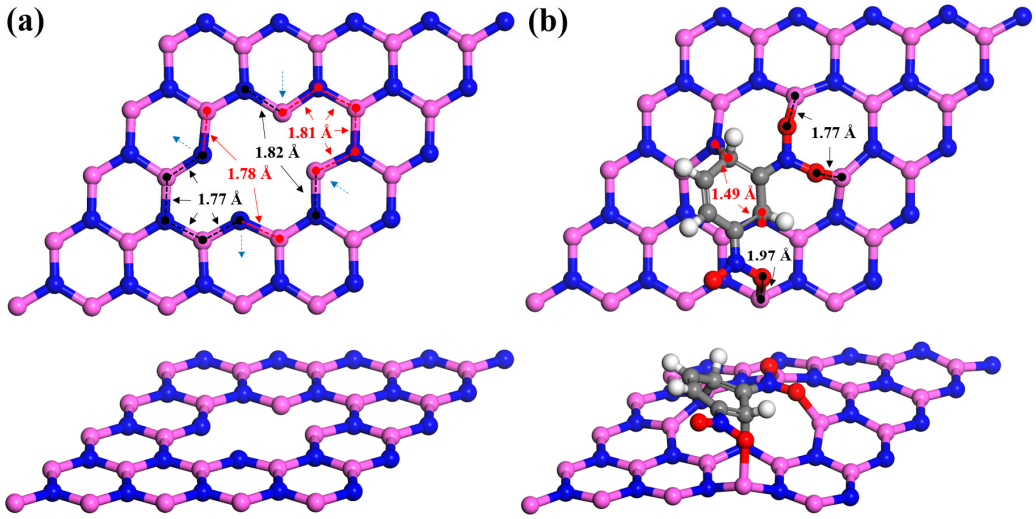

Figure 5. The optimized (**a**) AlN nanosheet with Al-N dual vacancies and (**b**) the most stable configuration after adsorption of m-DNB molecule.

The adsorption energy of m-DNB molecule on the above Al-N vacancy AlN nanosheet is −6.957 eV, which is 7.7 times than the value of pure AlN nanosheet. In order to understand the strong chemical interaction between m-DNB molecule and Al-N vacancy nanosheet, we studied the charge transfer between them as shown in Figure 6. A large number of charges agglomerate at the Al-O bond between the nitro group and the substrate. The nitro group also plays a role in promoting charge transfer and the charge exchange between the nitro group and the benzene ring is increased. The Bader charge analysis and PDOS in Figure 7 also confirmed this. The overall m-DNB molecule gets 1.397 e^- charges from the Al-N-vacancy AlN nanosheet, and the Al-p and O-p, C-p and N-p orbitals are obviously hybridized, respectively. According to the electronic density of states of Al-N-vacancy AlN nanosheet, it can be found that there is a new occupied state at the top of the valence band. Compared with pure AlN nanosheet, the band gap is reduced by about 0.3 eV. After adsorbing the m-DNB molecule, the top of the valence band and the bottom of the conduction band move down simultaneously, and the band gap value is sharply decreased from 2.372 eV to 1.682 eV. Unlike the case of pure AlN nanosheet, the band gap change is very significant in this system, which will affect the material's conductivity greatly and do good to the sensitivity of the signal in molecule sensing.

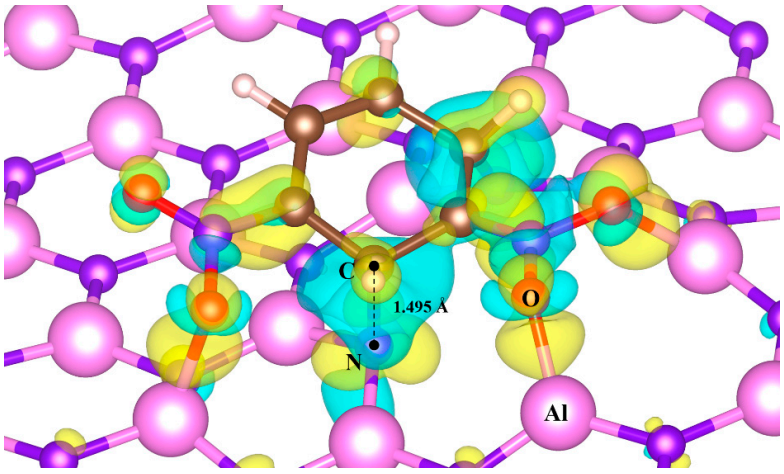

Figure 6. Differential charge density of m-DNB molecule adsorbed on AlN nanosheet with Al-N vacancies. The isovalue of charge density is 0.007 e/Å^3 (yellow: charge accumulation; cyan: charge depletion).

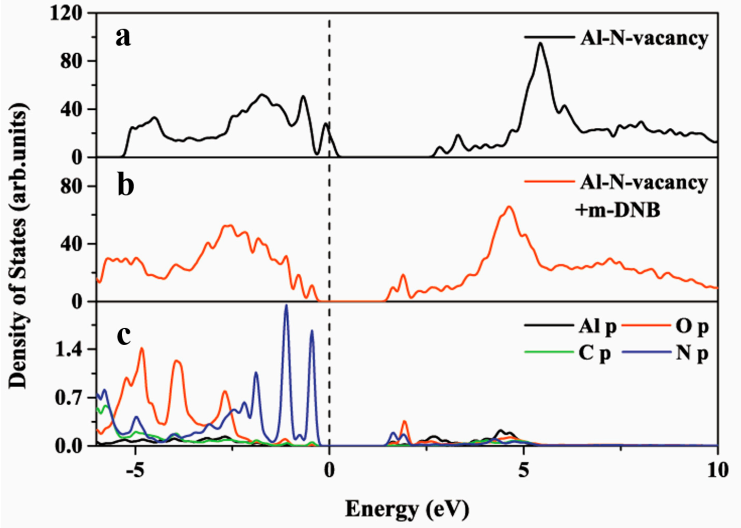

Figure 7. Electronic density of states of Al-N-vacancies AlN nanosheet before and after adsorption of m-DNB. (**a**) TDOS of Al-N-vacancy AlN nanosheet; (**b**) TDOS of Al-N-vacancy AlN nanosheet after the m-DNB molecule is adsorbed; (**c**) PDOS of O, C atom in m-DNB and neighboring Al, N atom in nanosheet. The Fermi energy is set to zero.

3.3. Interaction of m-DNB Molecule with Si-doped AlN Nanosheet

In order to evaluate the adsorption performance of Si-doped AlN nanosheet, firstly the model was relaxed. After geometric optimization, the structure of Si-doped AlN nanosheet was locally deformed near the Si atom, as shown in Figure 8. The introduction of Si atom causes the surrounding atoms to shrink toward the doping site, and the newly formed Si-N bond length is 1.69 Å which is smaller than the original Al-N bond length. When m-DNB molecule is adsorbed on the Si-doped nanosheet, the molecule is almost parallel to the substrate. The deformation only exists in a small part of the substrate. The O atom of the nitro group and the Al atom of the substrate form three approximately perpendicular Al-O bonds and bond lengths are 2.02 Å, 2.02 Å and 2.12 Å, respectively. The adsorption energy and adsorption distance are −3.360 eV and 2.02 Å, respectively, which are between the values of Al-N-vacancy nanosheet and pure AlN nanosheet, showing relatively moderate adsorption strength. It can be seen from the differential charge density in Figure 9 that the charge transfer is completely concentrated between the nitro group and the AlN nanosheet, and a large amount of charge is concentrated on the Al-O bond between m-DNB and Si-doped nanosheet. Meanwhile, the charge of the N-O bond is lost and the bond is weakened on the m-DNB molecule. The charge of 1.097 e^- was transferred from the Si-doped AlN nanosheet to the m-DNB molecule.

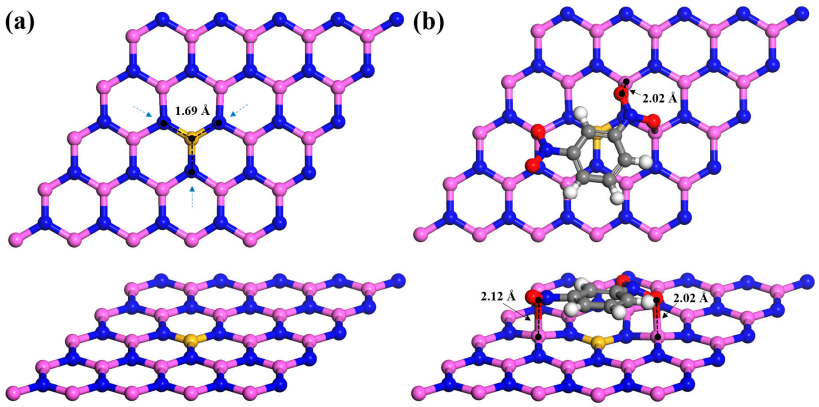

Figure 8. The optimized (**a**) Si-doped AlN nanosheet and (**b**) the most stable configuration after adsorption of m-DNB molecule.

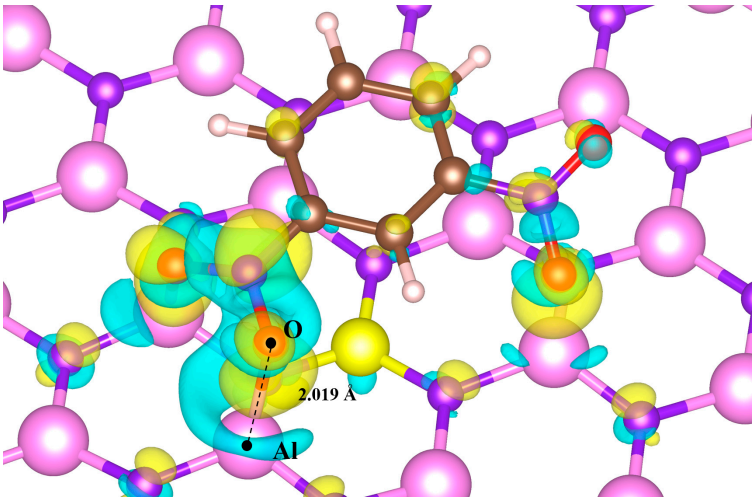

Figure 9. Differential charge density of m-DNB adsorbed on Si-doped AlN nanosheet. The isovalue of charge density is 0.003 e/Å^3 (yellow: charge accumulation; cyan: charge depletion).

In order to further understand the effect of Si-doping on the adsorption physics of m-DNB on AlN nanosheet, we have calculated the electronic density of states (DOS) before and after adsorption as shown in Figure 10. Due to the introduction of the Si atom, a potential energy level appears at the bottom of the conduction band and the AlN nanosheet transforms from the *p*-type to the *n*-type semiconductor. After adsorbing m-DNB molecule, the Fermi level returns from the bottom of the conduction band to the top of the valence band. The band gaps before and after molecular adsorption are 2.583 and 1.892 eV, which are the most obviously changed system among all modified nanosheets in this work. It would be very beneficial for m-DNB vapor sensing applications. It can also be seen that the O atom of the nitro group is hybridized with the Al atom of the surrounding substrate, which implies the good bond strength and corresponds well with the above charge transfer physics.

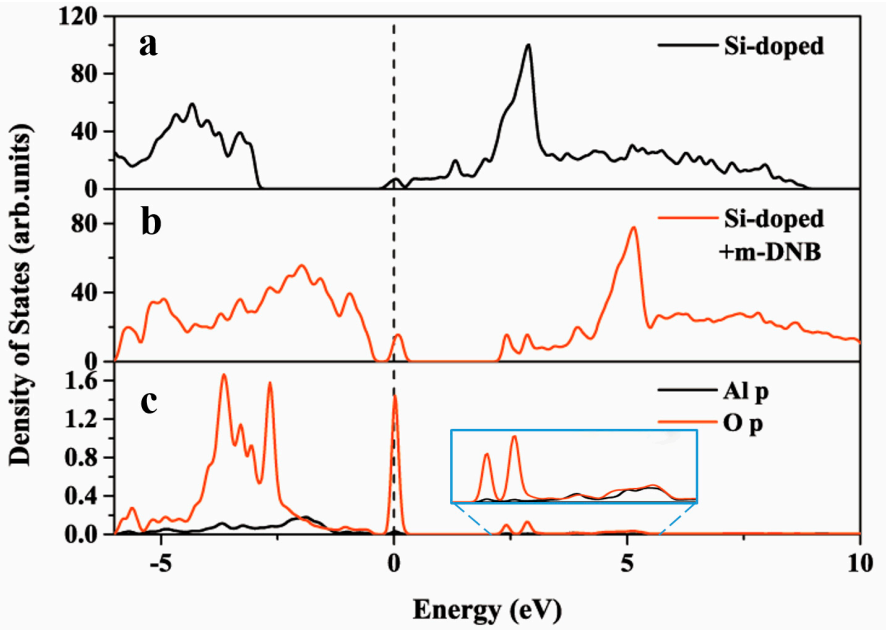

Figure 10. Electronic density of states of Si-doped AlN nanosheet before and after adsorption of m-DNB molecule. (**a**) TDOS of Si-doped AlN nanosheet; (**b**) TDOS of Si-doped AlN nanosheet after m-DNB adsorption; (**c**) PDOS of O atom in m-DNB and the neighboring Al, N atom in Si-doped AlN nanosheet. The Fermi level is set to zero.

4. Summary

In this work, we investigated the adsorption capability of pure, vacancy-containing and doped AlN nanosheets towards poisonous and explosive m-DNB for environmental safety applications from the perspective of DFT physics. Valuable results in terms of atomic structure, adsorption energy, differential charge density, charge transfer analysis and electronic density of states have been obtained to understand and predict the properties of materials. The AlN nanosheet with Al-N-vacancies is found to have large adsorption energy and the Si-doped AlN nanosheet has very obvious band gap change after m-DNB adsorption. The strong chemical interaction between Al-N-vacancies AlN nanosheet and m-DNB molecule, which makes the sheet more suitable as an adsorption or filtration material. The Si-doped AlN nanosheet with moderate adsorption energy and large change in band gap after m-DNB adsorption is a good candidate for this poisonous vapor sensing application.

Author Contributions: Formal analysis, H.Z., W.D., T.Z., R.A., Z.Q.; Project administration, Z.Q.; Supervision, Z.Q.; Writing—original draft, H.Z., W.D., Z.Q. All authors have read and agreed to the published version of the manuscript.

Funding: We are grateful for the support from the Natural Science Foundation of China (51801113), the Natural Science Foundation of Shandong Province (ZR2018MEM001), the Young Scholars Program of Shandong University (YSPSDU) and the Education Program of Shandong University (2020Y299). R.A. thanks the SNIC and HPC2N for providing the computing facilities.

Acknowledgments: The National Supercomputer Centre (NSC) and the HPC Cloud Platform of Shandong University are acknowledged.

Conflicts of Interest: The authors declare no conflict of interest.

References

1. Novoselov, K.S.; Geim, A.K.; Morozov, S.V.; Jiang, D.; Zhang, Y.; Dubonos, S.V.; Grigorieva, I.V.; Firsov, A.A. Electric field effect in atomically thin carbon films. *Science* **2004**, *306*, 666–669. [CrossRef]
2. Stankovich, S.; Dikin, D.A.; Piner, R.D.; Kohlhaas, K.A.; Kleinhammes, A.; Jia, Y.; Wu, Y.; Nguyen, S.T.; Ruoff, R.S. Synthesis of graphene-based nanosheets via chemical reduction of exfoliated graphite oxide. *Carbon* **2007**, *45*, 1558–1565. [CrossRef]
3. Prasongkit, J.; Amorim, R.G.; Chakraborty, S.; Ahuja, R.; Scheicher, R.H.; Amornkitbamrung, V. Highly sensitive and selective gas detection based on silicene. *J. Phys. Chem. C* **2015**, *119*, 16934–16940. [CrossRef]
4. Liu, C.; Feng, W.; Yao, Y. Quantum spin hall effect in silicene and two-dimensional germanium. *Phys. Rev. Lett.* **2011**, *107*, 076802. [CrossRef]
5. Liu, H.; Neal, A.T.; Zhu, Z.; Luo, Z.; Xu, X.; Tomanek, D.; Ye, P.D. Phosphorene: An unexplored 2D semiconductor with a high hole mobility. *ACS Nano* **2014**, *8*, 4033–4041. [CrossRef]
6. Song, L.; Ci, L.; Lu, H.; Sorokin, P.B.; Jin, C.; Ni, J.; Kvashnin, A.G.; Kvashnin, D.G.; Lou, J.; Yakobson, B.I.; et al. Large scale growth and characterization of atomic hexagonal boron nitride layers. *Nano Lett.* **2010**, *10*, 3209–3215. [CrossRef]
7. Golberg, D.; Bando, Y.; Huang, Y.; Terao, T.; Mitome, M.; Tang, C.; Zhi, C. Boron nitride nanotubes and nanosheets. *ACS Nano* **2010**, *4*, 2979–2993. [CrossRef]
8. Radisavljevic, B.; Radenovic, A.; Brivio, J.; Giacometti, V.; Kis, A. Single-layer MoS_2 transistors. *Nat. Nanotechnol.* **2011**, *6*, 147–150. [CrossRef]
9. Ganji, M.D.; Jameh-Bozorgi, S.; Rezvani, M. A comparative study of structural and electronic properties of formaldehyde molecule on monolayer honeycomb structures based on vdW-DF prospective. *Appl. Surf. Sci.* **2016**, *384*, 175–181. [CrossRef]
10. Schedin, F.; Geim, A.K.; Morozov, S.V.; Hill, E.W.; Blake, P.; Katsnelson, M.I.; Novoselov, K.S. Detection of individual gas molecules adsorbed on graphene. *Nat. Mater.* **2007**, *6*, 652–655. [CrossRef]
11. Safari, L.; Vessally, E.; Bekhradnia, A.; Hosseinian, A.; Edjlali, L. A density functional theory study of the sensitivity of two-dimensional BN nanosheet to nerve agents cyclosarin and tabun. *Thin Solid Film.* **2017**, *623*, 157–163. [CrossRef]
12. Kou, L.; Frauenheim, T.; Chen, C. Phosphorene as a superior gas sensor: Selective adsorption and distinct I–V response. *J. Phys. Chem. Lett.* **2014**, *5*, 2675–2681. [CrossRef] [PubMed]

13. Hussain, T.; Kaewmaraya, T.; Chakraborty, S.; Ahuja, R. Defect and substitution-induced silicene sensor to probe toxic gases. *J. Phys. Chem. C* **2016**, *120*, 25256–25262. [CrossRef]
14. Yuan, W.; Shi, G. Graphene-based gas sensors. *J. Mater. Chem. A* **2013**, *1*, 10078–10091. [CrossRef]
15. Dai, J.; Yuan, J.; Giannozzi, P. Gas adsorption on graphene doped with B, N, Al, and S: A theoretical study. *Appl. Phys. Lett.* **2009**, *95*, 232105. [CrossRef]
16. Lopez-Corral, I.; Piriz, S.; Faccio, R.; Juan, A.; Avena, M. A van der waals DFT study of PtH_2 systems absorbed on pristine and defective graphene. *Appl. Surf. Sci.* **2016**, *382*, 80–87. [CrossRef]
17. Lopez-Corral, I.; German, E.; Juan, A.; Volpe, M.A.; Brizuela, G.P. Hydrogen adsorption on palladium dimer decorated graphene: A bonding study. *Int. J. Hydrog. Energy* **2012**, *37*, 6653–6665. [CrossRef]
18. Basu, S.; Bhattacharyya, P. Recent developments on graphene and graphene oxide based solid state gas sensors. *Sens. Actuators B Chem.* **2012**, *173*, 1–21. [CrossRef]
19. Varghese, S.S.; Lonkar, S.; Singh, K.K.; Swaminathan, S.; Abdala, A. Recent advances in graphene based gas sensors. *Sens. Actuators B Chem.* **2015**, *218*, 160–183. [CrossRef]
20. Zhang, X.; Liu, Z.; Hark, S. Synthesis and optical characterization of single-crystalline AlN nanosheets. *Solid State Commun.* **2007**, *143*, 317–320. [CrossRef]
21. Li, Y.; Yang, Z.; Chen, Z.; Zhou, Z. Computational investigation on structural and physical properties of ain nanosheets and nanoribbons. *J. Nanosci. Nanotechnol.* **2010**, *10*, 7200–7203. [CrossRef] [PubMed]
22. Zhang, C.; Zheng, F. First-principles prediction on electronic and magnetic properties of hydrogenated AlN nanosheets. *J. Comput. Chem.* **2011**, *32*, 3122–3128. [CrossRef] [PubMed]
23. Valedbagi, S.; Fathalian, A.; Elahi, S.M. Electronic and optical properties of AlN nanosheet: An ab initio study. *Opt. Commun.* **2013**, *309*, 153–157. [CrossRef]
24. Zhang, C.; Wang, P.; Li, P.; Zheng, F. First-principles study on electronic structures and magnetic properties of AlN nanosheets and nanoribbons. *J. Appl. Phys.* **2012**, *111*, 094304. [CrossRef]
25. Ouyang, T.; Qian, Z.; Ahuja, R.; Liu, X. First-principles investigation of CO adsorption on pristine, C-doped and N-vacancy defected hexagonal AlN nanosheets. *Appl. Surf. Sci.* **2018**, *439*, 196–201. [CrossRef]
26. Du, W.; Zhao, C.; Liu, K.; Li, H.; Chen, Y.; Bai, Y.; Ahuja, R.; Qian, Z. Defective and doped aluminum nitride monolayers for NO adsorption: Physical insight. *Chem. Phys. Lett.* **2020**, *753*, 137592. [CrossRef]
27. Rastegar, S.F.; Hadipour, N.L.; Soleymanabadi, H. Theoretical investigation on the selective detection of SO_2 molecule by AlN nanosheets. *J. Mol. Model.* **2014**, *20*, 2439. [CrossRef]
28. Rastegar, S.F.; Peyghan, A.A.; Ghenaatian, H.R.; Hadipour, N.L. NO_2 detection by nanosized AlN sheet in the presence of NH_3: DFT studies. *Appl. Surf. Sci.* **2013**, *274*, 217–220. [CrossRef]
29. Rad, A.S.; Shabestari, S.S.; Jafari, S.A.; Zardoost, M.R.; Mirabi, A. N-doped graphene as a nanostructure adsorbent for carbon monoxide: DFT calculations. *Mol. Phys.* **2016**, *114*, 1756–1762. [CrossRef]
30. Nasehnia, F.; Seifi, M. Adsorption of molecular oxygen on VIIIB transition metal-doped graphene: A DFT study. *Mod. Phys. Lett. B* **2014**, *28*, 1450237. [CrossRef]
31. Li, F.; Shi, C. NO-sensing performance of vacancy defective monolayer MoS_2 predicted by density function theory. *Appl. Surf. Sci.* **2018**, *434*, 294–306. [CrossRef]
32. Ouyang, T.; Qian, Z.; Hao, X.; Ahuja, R.; Liu, X. Effect of defects on adsorption characteristics of AlN monolayer towards SO_2 and NO_2: Ab initio exposure. *Appl. Surf. Sci.* **2018**, *462*, 615–622. [CrossRef]
33. Chen, X.; Chen, B. Macroscopic and spectroscopic investigations of the adsorption of nitroaromatic compounds on graphene oxide, reduced graphene oxide, and graphene nanosheets. *Environ. Sci. Technol.* **2015**, *49*, 6181–6189. [CrossRef] [PubMed]
34. Nagarajan, V.; Chandiramouli, R. Investigation on probing explosive nitroaromatic compound vapors using graphyne nanosheet: A first-principle study. *Struct. Chem.* **2019**, *30*, 657–667. [CrossRef]
35. Bhuvaneswari, R.; Nagarajan, V.; Chandiramouli, R. Arsenene nanotube as a chemical sensor to detect the presence of explosive vapors: A first-principles insight. *J. Inorg. Organomet. Polym. Mater.* **2018**, *28*, 2844–2853. [CrossRef]
36. Zhang, J.R.; Yue, Y.Y.; Luo, H.Q.; Li, N.B. Supersensitive and selective detection of picric acid explosive by fluorescent Ag nanoclusters. *Analyst* **2016**, *141*, 1091–1097. [CrossRef]
37. Chandiramouli, R. Antimonene nanosheet device for detection of explosive vapors-A first-principles inspection. *Chem. Phys. Lett.* **2018**, *708*, 130–137. [CrossRef]
38. Kresse, G.; Furthmuller, J. Efficient iterative schemes for ab initio total-energy calculations using a plane-wave basis set. *Phys. Rev. B* **1996**, *54*, 11169–11186. [CrossRef]

39. Kresse, G.; Hafner, J. Ab-initio molecular-dynamics for open-shell transition-metals. *Phys. Rev. B* **1993**, *48*, 13115–13118. [CrossRef]
40. Kresse, G.; Hafner, J. Ab-initio molecular-dynamics simulation of the liquid-metal amorphous-semiconductor transition in germanium. *Phys. Rev. B* **1994**, *49*, 14251–14269. [CrossRef]
41. Kresse, G.; Furthmuller, J. Efficiency of ab-initio total energy calculations for metals and semiconductors using a plane-wave basis set. *Comput. Mater. Sci.* **1996**, *6*, 15–50. [CrossRef]
42. Kresse, G.; Joubert, D. From ultrasoft pseudopotentials to the projector augmented-wave method. *Phys. Rev. B* **1999**, *59*, 1758–1775. [CrossRef]
43. Perdew, J.P.; Burke, K.; Ernzerhof, M. Generalized gradient approximation made simple. *Phys. Rev. Lett.* **1996**, *77*, 3865–3868. [CrossRef] [PubMed]
44. Blochl, P.E. Projector augmented-wave method. *Phys. Rev. B* **1994**, *50*, 17953–17979. [CrossRef]
45. Monkhorst, H.J.; Pack, J.D. Special points for brillouin-zone integrations. *Phys. Rev. B* **1976**, *13*, 5188–5192. [CrossRef]
46. Grimme, S. Semiempirical GGA-type density functional constructed with a long-range dispersion correction. *J. Comput. Chem.* **2006**, *27*, 1787–1799. [CrossRef]
47. Beiranvand, R.; Valedbagi, S. Electronic and optical properties of advance semiconductor materials: BN, AlN and GaN nanosheets from first principles. *Optik* **2016**, *127*, 1553–1560. [CrossRef]